Journal of Fusion Energy (2022)41:7
https://doi.org/10.1007/s10894-022-00319-7

ORIGINAL RESEARCH

The Magnetized Indirect Drive Project on the National Ignition Facility

J. D. Moody[1] · B. B. Pollock[1] · H. Sio[1] · D. J. Strozzi[1] · D. D.-M. Ho[1] · C. Walsh[1] · G. E. Kemp[1] · S. O. Kucheyev[1] · B. Kozioziemski[1] · E. G. Carroll[1] · J. Kroll[1] · D. K. Yanagisawa[1] · J. Angus[1] · S. D. Bhandarkar[1] · J. D. Bude[1] · L. Divol[1] · B. Ferguson[1] · J. Fry[1] · L. Hagler[1] · E. Hartouni[1] · M. C. Herrmann[1] · W. Hsing[1] · D. M. Holunga[1] · J. Javedani[1] · A. Johnson[1] · D. Kalantar[1] · T. Kohut[1] · B. G. Logan[1] · N. Masters[1] · A. Nikroo[1] · N. Orsi[1] · K. Piston[1] · C. Provencher[1] · A. Rowe[1] · J. Sater[1] · K. Skulina[1] · W. A. Stygar[1] · V. Tang[1] · S. E. Winters[1] · J. P. Chittenden[2] · B. Appelbe[2] · A. Boxall[2] · A. Crilly[2] · S. O'Neill[2] · J. Davies[3] · J. Peebles[4] · S. Fujioka[5]

Accepted: 4 April 2022

Abstract
A new project is underway at the National Ignition Facility with the goal of applying a seed magnetic field to the fusion fuel in an indirect drive hohlraum implosion and quantifying the effect on the hot-spot temperature, shape and neutron yield. Magnetizing fusion fuel is calculated to reduce heat loss from the implosion core by constraining the motion of electrons and fusion-generated alpha particles; this can improve the chances of achieving high-gain fusion in a laboratory plasma. We describe the goals of this project and the significant scientific and technological challenges which must be overcome for this project to succeed.

Keywords Inertial confinement fusion · Indirect drive · Magnetized ignition · National IgnitionFacility

Introduction

Creating and maintaining self-sustaining nuclear fusion reactions in the laboratory, such that energy output exceeds energy input, continues to challenge physicists worldwide. Indirect drive inertial confinement fusion (ICF) experiments on NIF have recently obtained a nuclear energy output which is $\sim$ 5 times the energy coupled into the fusion fuel and some recent experiments have achieved a burning plasma [1–4]. A burning plasma occurs when the total fuel re-heating energy from alpha particles generated in deuterium–tritium (DT) nuclear reactions exceeds the total mechanical (PdV) work done to assemble the hot-spot. Ignition occurs when the self-heating overpowers all loss mechanisms and the temperature rises in an increasing "explosive" fashion. These results are very encouraging and suggest that self-sustaining nuclear fusion in the laboratory is nearly within hand. Once laboratory fusion is achieved remaining challenges include understanding burning plasma physics, creating implosion designs which achieve higher fusion energy gain and increasing margin and robustness in the current designs. Margin offers the possibility of making trade-offs between design choices that can make ignition easier.

Pre-magnetizing the DT fuel with a seed field in the range of $\sim$40 T is an idea that has been around since the 1950s [5] and offers the possibility of increasing performance, margin and robustness of ICF designs, even if they have reached the burning plasma regime [6]. This paper describes an ongoing project at NIF to magnetize the fusion fuel in an ICF implosion [7, 8] and presents the technological challenges and the design choices made for the NIF project. The project goal is to pre-magnetize the deuterium–tritium fuel in a hohlraum target to $\sim$40 T prior to firing the NIF laser which initiates the implosion. This

✉ J. D. Moody
moody4@llnl.gov

1 Lawrence Livermore National Laboratory, Livermore, CA 94550, USA

2 Imperial College, London, UK

3 University of Rochester, New York, USA

4 Laboratory for Laser Energetics, New York, USA

5 Institute for Laser Engineering, Osaka, Japan

requires developing a cryogenic pulsed-power capability, inventing a new high-resistivity hohlraum material, developing new DT ice layer thermal control methods, using target physics models to innovate a new magnetized implosion design and performing target physics experiments to quantify the magnetization effects on implosion performance. The outline of the rest of this paper is as follows: "Approaches to Laboratory Fusion" section reviews several methods for achieving laboratory fusion and describes some of the important physics considerations for magnetized ICF. "Previous and Current Work on Magneto-inertial Fusion" section reviews the history and current status of magnetized ICF fusion efforts. "Magnetization Considerations and General Criteria" section describes the technological challenges for the NIF magnetized ICF project; "Future Plans" section describes the planned NIF experiments and "Conclusions" section presents conclusions.

Approaches to Laboratory Fusion

Figure 1 shows three approaches to laboratory fusion and indicates their differences in terms of the range of plasma β and the Hall parameter, χ. Magnetized plasma systems are generally characterized by these two parameters defined as

$$\beta = \frac{nT}{B^2/(2\mu_0)}, \tag{1}$$

$$\chi = \omega_{ce}\tau_{ei}. \tag{2}$$

In these expressions, n is the plasma electron density, T is the plasma electron temperature expressed in energy units, B is the magnetic field amplitude, μ_0 is the free space permeability, $\omega_{ce} = eB/m_e$ is the electron cyclotron frequency, e is the elementary charge, m_e is the electron mass,

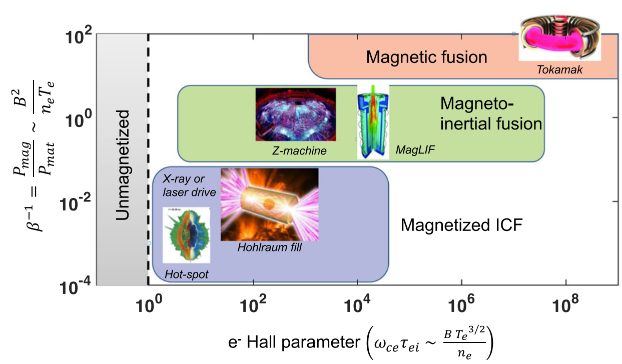

Fig. 1 Three approaches to laboratory fusion are shown according to the effect of the magnetic field on transport (the Hall parameter) and the relative importance of the magnetic field on plasma dynamics given in terms of the plasma "beta"

$\tau_{ei} = \frac{3\sqrt{m_e}(T)^{3/2}}{4\sqrt{2\pi}n\lambda e^4}$ is the electron-ion collision time and λ is the Coulomb logarithm. The plasma β is the ratio of thermal pressure to magnetic pressure and if close to unity indicates that the particles and field are equally important in the plasma dynamics. The Hall parameter describes the effect of the magnetic field on transport parameters. When $\chi > 1$ the electron mean-free-path becomes limited to the Larmour radius provided that it is less than the unmagnetized electron-ion collisional mean-free-path. The consequence of this is that particle and energy transport can be significantly reduced perpendicular to the local magnetic field direction. The classical Braginskii transport coefficients [9] are written with explicit dependence on χ and show that for $\chi > 1$ transport across the magnetic field is reduced. Along the field the transport is unchanged. Sadler gives a recent discussion of the parametric space for magnetized high-energy-density plasma [10]. He points out that the "ram pressure" due to plasma flow should be included in the plasma pressure when the Mach number is not small.

Magnetic Confinement Fusion (MCF) plasma systems [11], which include tokamaks, stellarators and reversed-field pinches [12], typically have a particle energy density (thermal pressure) smaller than the magnetic energy density so that $\beta < 1$. This means that the plasma remains confined as long as the magnetic field is confined and the instabilities that cause cross-field transport are minimized and controlled. The Hall parameter is typically large in these systems so that the electrons are magnetized, and heat and particle transport across the B-field direction is significantly reduced relative to along the field direction.

In contrast to MCF plasmas, magnetized ICF hot-spot plasmas typically have β in the range of 40 to 100 which means that the high density plasma effectively "pushes around" the magnetic field. Simulations show that χ is 2 to 5 in the hot-spot and $\gg 1$ in regions of the hohlraum plasma so that the field suppresses electron thermal transport perpendicular to the magnetic field direction.

Several research groups are developing the fusion approach knows as magneto-inertial fusion (MIF) which is in the parameter regime in Fig. 1 that lies between magnetized ICF and MCF. Research efforts on this topic include the MagLIF project at Sandia National Laboratory (SNL) [13, 14], the mini-MagLIF project at the Laboratory for Laser Energetics (LLE) [15, 16], the dense plasma focus system [17, 18] at several National Laboratories in the US and the shear stabilized Z-pinch at the University of Washington [19]. The interested reader is referred to the references listed for these projects as well as Lindemuth's article on MIF [20].

The Lawson Condition for Magnetized ICF

The Lawson condition [21, 22] consists of a simple product of fuel density, n, and energy confinement time, τ_E, which must exceed a minimum threshold value to achieve self-sustaining fusion burn or *ignition*. Lawson originally derived the condition by requiring that the sum of the input power and plasma heating power from fusion products equals or exceeds the sum of the radiative and conduction power losses from the plasma. Since the original paper, the Lawson criterion has been recast as an $nT\tau_E$ product with T being the plasma temperature.

The Lawson condition has been extended to ICF and is typically expressed in terms of the "p-τ" product where p is the hot spot pressure and τ is the time that the hot spot remains in a compressed core at stagnation before the high pressure causes the hot spot to expand and fall apart [23–25]. In a uniform plasma with $n = n_i = n_e$ and $T = T_i = T_e$ (where the subscripts i and e correspond to ion and electron quantities) the different expressions for the Lawson condition are related as $p\tau = 2nT\tau_E$. For a 50-50 D-T plasma a threshold for $nT\tau$ of 4.6×10^{14} s keV/cm^3 at $T = 14$ keV is required for ignition [26]. The p-τ product is not useful in practice since it is given as the product of two quantities which must be inferred from other measurements. It is more useful to express the generalized Lawson criterion (GLC) in terms of the hot spot temperature, T, and the areal fuel density, ρR, which is the integral of the fuel density along the radial direction [27]. Specifically, this results in a threshold condition on ρRT^2 [28]. Neutron energy spectra give a measure of T and the value of ρR and can be obtained from secondary neutrons or initial conditions of the DT fuel in the capsule and the hot-spot shape from X-ray measurements.

An approximate condition for a magnetized self-sustaining burning ICF plasma can be constructed by starting with the power balance in the unmagnetized hot spot [29, 30]. The rate of change of the hot-spot internal energy is $dE/dt = P_F - P_M - P_r - P_e$, where E is the hot spot energy, P_F is the fusion power as defined earlier, P_M is the mechanical power, P_r is power lost by radiation, and P_e is power lost through electron thermal conduction. In general there is an additional loss term from mix which depends on the compression which has not been included in this description. At stagnation we set the mechanical power to zero and then look for the hot-spot conditions that give $dE/dt \geq 0$. All the remaining terms can be expressed as functions of ρR and T, giving

$$\rho R[\mathrm{g/cm^2}] \geq \left[\frac{10^{-4} f_e T^{7/2}}{10^{17}\langle\sigma v\rangle f_\alpha - 0.385 T^{1/2}}\right]^{1/2}, \tag{3}$$

where $0 < f_e \leq 1$ is a multiplication factor which approximates effects that modify the electron thermal conduction (such as magnetic fields), T is the hot spot temperature in keV and f_α is the fraction of alpha particle energy which reheats the hot spot; typically, $f_\alpha \sim 0.75$. The reaction cross-section, $\langle\sigma v\rangle$, is only a function of T and can be estimated using the improved formula from Bosch and Hale [31]. The bracketed term in Eq. (3) must be non-negative and shows that there is a minimum value of $T =$ 4.3 keV for $f_\alpha = 1$. If the hot-spot temperature falls below this minimum value then radiation losses exceed heating from the nuclear reaction products and a self-heating hot-spot is not possible.

Applying a magnetic field to the fuel which is large enough to fully magnetize the electrons in the hot-spot ($\chi \gg 1$) effectively reduces the electron thermal conduction to a fraction, f_e, of the unmagnetized value. For a spherical hotspot, the minimum $f_e = 0$ occurs for a purely azimuthal B-field where the field lines are closed. A simple axial current or more complex current topologies have been suggested for achieving closed field lines [33]. For now, we consider a purely axial, z-directed field. Typically an initial B_z develops a radial component as the implosion proceeds, so a pure B_z in the hot-spot is unrealistic. However, an axial field gives the smallest f_e for a field with no azimuthal component.

The value of f_e to use for a magnetized implosion can be estimated by considering the B-field induced reduction to the electron thermal energy just due to conduction: $\partial_t U_e = -\nabla \cdot \mathbf{q}_e$ with heat flux $\mathbf{q}_e = -\overleftrightarrow{\kappa} \cdot \nabla T_e$ and conductivity tensor $\overleftrightarrow{\kappa}$. The total power loss from a sphere is $P_e = -\oint \mathbf{q}_e \cdot d\mathbf{A}$, integrated over its surface. For a purely radial temperature variation and an axial field, $f_e = P_e(B)/P_e(B=0) = 1/3 + (2/3)\kappa_\perp/\kappa_{||}$ where $\kappa_{||}$ is the unmagnetized value and $\kappa_\perp$ is perpendicular to $\mathbf{B}$. Note that the Righi–Leduc $\kappa_\wedge$ contribution vanishes for our geometry. For $\chi \gg 1$, $\kappa_\perp/\kappa_{||} \to 0$ and $f_e \to 1/3$.

The approximate effect of magnetization on the hot-spot parameters for a good performing NIF implosion such as NIF shot N170601 [34] is shown in Fig. 2. This figure shows a group of DT layered implosions performed on NIF over eight years, plotted according to their ion temperature and core areal-density values [32]. The dotted gray line shows the boundary calculated for a self-heating hot spot according to Eq. (3) where $f_\alpha = 0.75$ (typical of NIF implosions) and $f_e = 1$ corresponding to no applied B-field. An igniting plasma, which undergoes runaway self-heating, must be to the right and above this boundary. Shot N170601 is identified in Fig. 2 as the red point at $T = 4.56$ keV and $\rho R = 0.256$ g/cm^2. Simple scaling formulas derived by Hurricane [32] show that if the electron thermal

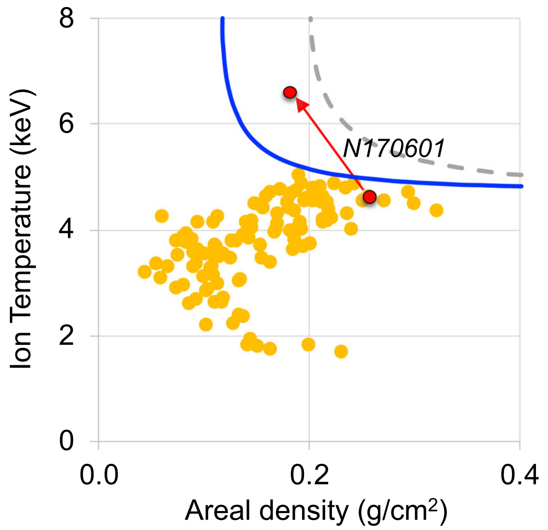

Fig. 2 Ion temperature versus areal density for eight years of NIF DT layered implosions from 2010 to 2018 [32]. The curves indicate the threshold beyond which a self-heating plasma is achieved with fuel magnetization (solid blue line) and without fuel magnetization (dashed gray line). Simple scaling calculations show how a 30-T seed field would change the hot-spot conditions for shot N170601 (red dots) (Color figure online)

conductivity is reduced to $1/3$ of its classical value then the ion temperature increases by approximately $3^{1/3}$ and the ρR value changes by $3^{-1/3}$. This places the magnetized version of N170601 at $T = 6.57$ keV and $\rho R = 0.18$ g/cm^2. Decreasing f_e from 1 to $1/3$ in Eq. (3) causes the dotted gray line to shift to the blue line plotted in Fig. 2. The effect of magnetization on the Lawson condition is to reduce the ρR required for a self-heating hot-spot to $1/\sqrt{3}$ of the unmagnetized value at the same T, allowing for designs with less hot-spot compression. The expected hot-spot conditions of magnetized N170601 is shown in Fig. 2 as the second red point which now sits squarely in the self-heating hot-spot region. Note that the increase in T_{ion} also causes a decrease in areal density for the same drive because of the higher hot-spot backpressure. A consequence of this reduced areal density is a reduction in the slowing down of the alpha particles, f_α. However, the compression-amplified hot-spot magnetic field is large enough to trap the alpha particles increasing their energy deposition; this recovers most of the reduction in f_α [35, 36].

Capsule-only radiation-magnetohydrodynamic simulations with the Lasnex code [37, 38] approximately reproduce the simple scaling of the hot-spot conditions at stagnation when applying a B-field [39]. The unmagnetized simulation uses a small level of fuel preheat to approximate the sources of experimental degradations and match the data. Using the same preheat degradation for a magnetized simulation shows a hot-spot trajectory that reaches stagnation parameters close to the simple scaling estimates for T and ρR for the magnetized version of N170601.

Previous and Current Work on Magneto-inertial Fusion

The idea of combining inertial and magnetic confinement dates back at least to 1962 and the work of George Linhart, who proposed using it with explosive drivers [5]. Over the next several decades, as laser, particle-beam, impact, and other drivers were developed, researchers proposed adding magnetic fields to fuel volumes in these systems as well [40–42]. The idea is that, according to the “frozen-in law” of magnetohydrodynamics, an initial seed magnetic field can be amplified enormously as the plasma-and consequently the magnetic field-is compressed. Experiments show that an initial shock generated by the X-ray drive preheats the fuel converting it to a low temperature plasma with high conductivity which then “locks” the magnetic field into the fuel. Behind the shock, the inward advancing ablator and fuel compress the fuel ahead of it as the shock converges in 2D (cylindrical) or 3D (spherical) geometry. Without a shock there would need to be another source to significantly increase the material’s electrical conductivity.

Magnetized ICF schemes have been explored extensively using radiation magneto-hydrodynamic simulation tools [6, 43–46] but the experimental study is still in its early stages [33, 47–49]. Modeling of an applied seed magnetic field in the DT fuel of an ICF implosion shows that the internal B-field flux remains approximately conserved during the implosion. This leads to amplification of the hot-spot B-field by the factor C_R^2 where C_R is the convergence ratio or the initial outer radius of the fuel divided by the final fuel radius at stagnation. Scaling estimates based on an adiabatic hot-spot compression give $\chi \sim C_R^2$ and $\chi > 1$ throughout the implosion. In addition to magnetizing the electrons, the amplified B-field causes the Larmour radius of the 3.5 MeV alpha particles generated through D-T fusion reactions to be smaller than the hot spot size so the alphas become trapped and stay in the hot-spot for longer time. Both effects lead to a higher temperature hot-spot and the potential to boost marginally igniting designs to the runaway self-heating regime. The simulations also show the potential of the hot-spot B-field to mitigate certain short scalelength Rayleigh–Taylor instabilities that can generate mix between the ablator and fuel and degrade the implosion [6, 43, 46]. Applying a seed field to a high fusion gain design or one that is significantly far from self-heating does not substantially improve the implosion performance; the magnetic field is most effective at pushing designs close to the ignition boundary over the boundary.

Typically, there is a non-zero resistivity to the fuel-ablator plasma which allows the compressed field to diffuse into the lower field regions. The extent of this diffusion is characterized by the magnetic Reynolds number, which is expressed as

$$R_m = \mu_0 \sigma v L. \tag{4}$$

Here, v is a characteristic plasma velocity, L is a characteristic size of a plasma structure, σ is the plasma conductivity, and μ_0 is the permeability of free space. If R_m is of order unity or smaller, then the magnetic field diffuses away too quickly to affect the implosion; if R_m is large, then the magnetic field will remain frozen into the plasma. For a typical NIF ICF implosion, $v \sim 200$ km/s, $L \sim 50$ µm and the material is cold until heated by the first shock. The plasma resistivity for $Z = 1$ and a Coulomb logarithm of 5 is approximately $\rho = \frac{1}{\sigma} \sim 15.2\,\mu\Omega\text{-cm}\ \ (100\ \ \text{eV}/T_e)^{3/2}$ giving $R_m \sim 100(T_e/100\,\text{eV})^{3/2}$. Since the capsule does not converge much before the shocks break out into the DT fuel, the field will be frozen into the hotspot as it implodes if the shocks heat it to above 30 eV, which they typically do.

The Nernst effect [9, 50] entails the advection of magnetic field by the heat-carrying electrons toward lower temperature. In an ICF implosion the thermal gradient tends to be radially outward for much of the implosion time, so the Nearnst effect may increase the B-field in the central hot-spot.

Recent laboratory experiments using magnetized fusion fuel by the US National ICF Program have shown promising results. Starting in 2010, researchers at the Laboratory for Laser Energetics (LLE) at the University of Rochester, New York, successfully demonstrated magnetic compression in a cylindrical direct-drive implosion [48] with a seed B-field of 8 T aligned primarily along the cylinder axis. Proton deflection measurements indicated a core B-field of about 4 kT which was roughly consistent with an amplification of the seed field by the expected C_R^2. This was followed in 2011 by the first magnetized laser direct-drive spherical implosion experiment [33, 49] with a seed B-field of 8 T. In broad accordance with model predictions, they achieved a modest but observable 15% increase in ion temperature and a 30% increase in neutron yield.

Several years later in 2014, magnetized fuel was tested as part of the Magneto-Inertial Magnetic Direct Drive (MI-MDD) program at the Sandia National Laboratory, Albequerque, New Mexico. This experiment employed the MagLIF (Magnetized Liner Inertial Fusion) approach, a magneto-inertial fusion scheme which uses the inward directed Lorentz force generated by an intense current through a cylindrical metal liner to rapidly compress the enclosed fuel [44]. The team compared MagLIF's baseline performance with configurations in which the deuterium fuel was both magnetized and laser preheated. With both of these additional conditions, the experiment achieved a roughly threefold increase in plasma temperature and a 200-fold increase in neutron yield [13, 14]. Cylindrical implosions are a continued area of study focusing on the "mini MagLIF" target [15, 16].

In 2015, scientists at LLNL started a three-year project to lay the groundwork for magnetized indirect-drive experiments on the NIF [6, 43]. The theoretical part of this work showed that implosions close to triggering a fusion burn can be pushed over the threshold with a 50 T seed field pre-imposed in the fuel. Hohlraum modeling of magnetized targets with high hohlraum gas-fill density showed a modest increase in the plasma temperature, with higher T_e and lower n_e in the equatorial channel between capsule blowoff and high-Z wall offering the prospect of improved inner-beam propagation. This work also found that the field could guide hot electrons generated by laser-plasma instabilities to the capsule and increase their deposition in the DT fuel, depending on when and where the electrons are produced [51]. The experimental part of this project developed a pulsed-power system consisting of a 4 µF capacitor that is charged to 40 kV and uses a spark gap switch and a low inductance stripline with a rise time of several microseconds when driving current through a solenoidal copper coil. Figure 3 shows a simplified schematic of the first pulser system currently used to magnetize targets on NIF and which is very similar to the original pulser tested only in the laboratory [6]. The resistance is a single lumped element representation of the total resistance in the current path including the hohlraum coil and the inductance includes both the hohlraum coil (about 100 nH) and the stripline inductance. During the lab pulser tests, experimenters applied the pulsed-power system to a coil

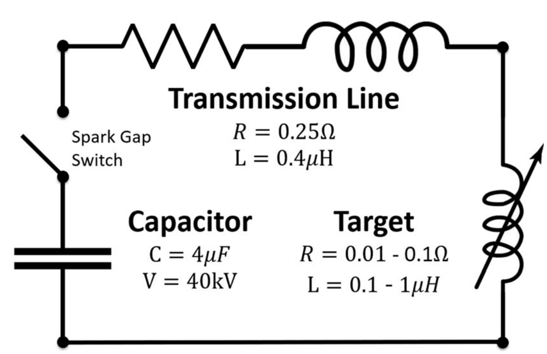

Fig. 3 Simplified schematic shows the fast pulser system developed for magnetizing NIF targets

wound around a high-Z metal cylinder with a measured electrical resistivity of 50 μΩ-cm and measured 50 T using a B-dot probe placed inside the cylinder. This provided an existence proof for being able to diffuse an imposed B-field through a high-Z hohlraum and into the region which would contain the fuel. More recent studies, discussed below, show that a hohlraum with electrical resistivity above 100 μΩ-cm is required for the cryo magnetized hohlraum. A second NIF pulser is currently under construction which will be used to magnetized DT cryo-layered implosions. This new system will be placed outside of the target area to increase neutron shielding and will be capable of reaching 60 T.

Also in 2015 Montgomery [52] demonstrated improved coupling to a hohlraum plasma using the Omega laser at the Laboratory for Laser Energetics. The experiment found that applying a 7.5 T B-field to a gold hohlraum with a 5 micron thick wall and a CH gas-fill increased the hohlraum plasma temperature from 3.6 to 4.6 keV or about 30%. The measurements were made using the optical Thomson scattering instrument.

A second three-year project at LLNL started in 2019 with the goal of demonstrating key scientific elements of magnetized NIF implosions experimentally [7, 8]. The project focuses on quantifying the magnetic field effects on room temperature gas-filled capsule implosions (not ice layered). In addition, it develops the method for implementing magnetized fuel on cryogenically layered DT implosions. If the magnetized room-temperature NIF implosions show close to the simulated performance improvement, then this technology for applying a seed magnetic field to DT fuel will be made available to augment any DT implosion design on NIF. The results will inspire future design options that combine magnetic and inertial confinement fusion physics to possibly achieve high fusion-energy gain.

Magnetization Considerations and General Criteria

Magnetizing a cryo fuel layer in an indirect drive hohlraum requires overcoming a number of significant scientific and technological challenges which are summarized in a set of requirements listed in Table I. A sketch of the magnetized room temperature hohlraum target planned for use on NIF is shown in Fig. 4a. Visible on the outside of the hohlraum is the solenoidal coil of insulated copper wire. The following sections discuss each requirement in the table, providing further description and implications.

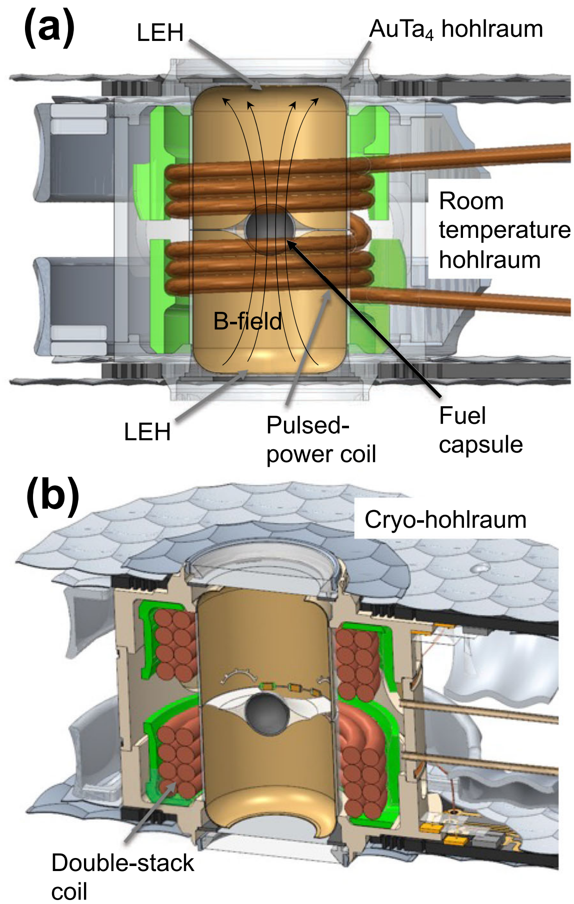

Fig. 4 **a** Sketch shows the magnetized room temperature Au:Ta hohlraum with a solenoid coil for magnetizing the fuel; LEH is the laser entrance hole. **b** Sketch of the magnetized cryogenic hohlraum target design which uses a double-stack coil to achieve higher magnetic fields

Induction Voltage Breakdown Considerations

Requirement 1 is important for successfully magnetizing the DT fuel. Tritium decay in the DT fuel creates β-particles (electrons) with an average energy of 5.7 keV [53]. These primary electrons collide on D and T (either in the gas or ice) and create secondary electrons. The increase of the B-field during magnetization and the induced loop voltage in the fuel vapor has the potential to trigger an avalanche breakdown creating a plasma with sufficient conductivity that it could exclude the B-field from soaking into the entire fuel volume. An estimate shows that this is very unlikely. Each beta decay electron generates about 165 secondary electrons as it collisionally slows down loosing about 34.6 eV each time it ionizes a D or T. The beta decay rate per tritium atom is 1.782×10^{-9}/s. For a 50:50 D-T gas near the triple point the vapor pressure is about 600 Torr at $\sim$ 18 K which gives an electron density of 2.9×10^{20}/cm^3. Near the edge of the capsule the magnetically generated electric field for the fast pulser shown in Fig. 3 is about 75 V/cm. The reduced electric field is given by $E/n_e = 75/2.9 \times 10^{20} \times 1 \times 10^{17} = 0.026$ Td, where the unit is Townsend = V-cm^2. Note that the reduced electric field value is smaller in the solid. The reduced electric field needs to reach about 100 Td for avalanche breakdown so the DT vapor is far from this. This consideration does not prohibit use of a fast pulser.

Diamagnetic Considerations

Requirement 2 limits the potential degradation of the B-field from diamagnetic effects. The HDC (High Density Carbon) capsule and DT fuel are both diamagnetic. This means that in the relation $B = \mu H = \mu_0(1 + \chi_m)H$ $\chi_m < 0$ for a diamagnetic material. The diamond shell has $\chi_{HDC} = -2.1 \times 10^{-5}$ and for solid DT at a density of 0.2 g/cm^3, $\chi_{DT} = -2.5 \times 10^{-6}$. Jackson [54] gives a solution for the field inside a shell with magnetic susceptibility. Approximating the effect on the field using only the HDC ablator (since χ_{HDC} is about 10x of χ_{DT}) we find that the field at the center of the capsule is $B(r = 0) \sim B_0\hat{z}\left(1 - \frac{2}{3}\chi_{HDC}^2\frac{\Delta}{a}\right)$ where Δ is the HDC shell thickness and a is the shell inner radius. Estimating the effect we find that the change in the central field is about $\Delta B/B \sim -2 \times 10^{-11}$ which is negligible. Most materials except for superconductors have a value of χ_m within a factor of 50 of the HDC value. This is the case for other ablator materials such as CH or Be which will also give a negligible change in the applied B-field. Note that a Be capsule is only viable provided it has a sufficiently low electrical conductivity.

Hohlraum Material

Estimates show that a Au hohlraum cannot meet Requirements 3-5 if used with the fast pulser. The field soak-through process in a conducting cylinder (good approximation to a hohlraum) is diffusive with an e-fold diffusion time given by $\tau = \mu_0\sigma R\delta/2$, where σ is the material conductivity which depends on the material temperature, R is the cylinder radius and δ is the wall thickness. The soak through time is about 2.5 µs for a typical gold hohlraum with $R = 2.7$ mm and $\delta = 30$ µm. The eddy currents in the gold wall generate Ohmic heating increasing the temperature by [8]

$$\Delta T = \frac{B_0^2}{2\mu_0}\frac{R\omega\tau}{\delta\rho_m C_p}\frac{\pi}{4} \tag{5}$$

where ρ_m is the material mass density, C_p is the specific heat and $t_{peak} = \pi/(2\omega)$ is the time to reach peak magnetic field. Note that ΔT is independent of the wall thickness (since τ/δ is independent of δ) but is linearly dependent on ω showing that a slower pulser rise-time leads to a lower temperature increase. If the change in material temperature is significant the dynamics of B-field soak-in must include the temperature-dependent resistivity A fast pulser with a several microsecond B-field ramp-up time will heat the gold wall to melt temperature for $B_0 \geq 10$ T. Estimates as well as detailed simulations of the field soak-in time, wall temperature increase and wall motion which include the temperature-dependent Au resistivity are shown in Ref. [8].

Figure 5a shows the time-dependent B-field measured with a B-dot probe placed inside a solenoidal coil compared with the B-field inside a 10 micron thick Au cylinder placed inside the solenoidal coil. Each of these cases was tested with a fast 2.5 µs rise-time pulser. The field inside the Au cylinder shows an initial delay relative to the case without the Au cylinder. Then, the B-field inside the Au cylinder catches up and reaches the same peak field as the coil without the Au cylinder. The reason for this is that eddy currents heat the wall causing the resistivity to increase and this allows the B-field to soak in more quickly. Even though the field soak-through is acceptable in this case the hohlraum wall temperature increase and wall motion exceed the requirements in Table 1.

The hohlraum wall is allowed to move up to 50 µm before the location of the NIF lasers on the hohlraum wall move enough to change the symmetry of the X-ray drive on the capsule resulting in a significant implosion asymmetry [55]. During magnetization the difference between the B-field on the outside and inside of the hohlraum generates inwardly directed radial magnetic forces which apply inward pressure on the hohlraum. If the inward pressure exceeds the mechanical buckling pressure the hohlraum

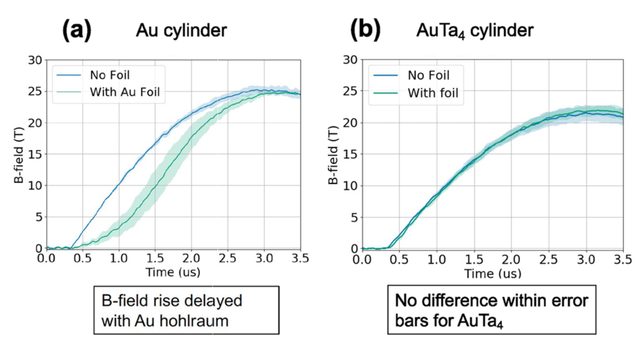

Fig. 5 **a** Plot shows that the B-field measured with a B-dot probe on the inside of a Au cylinder is delayed due to the soak-in time through Au when compared with the B-field without the Au. **b** Plot shows the B-field measured inside a $AuTa_4$ cylinder is nearly indistinguishable from the B-field measured with no cylinder. The band around each line corresponds to the measurement error bars

Table 1 Requirements for the pulser-target system

Num.	Description	Requirement	Comments
1	Limit to $\partial B/\partial t$	Precludes avalanche breakdown in DT	For all internal hohlraum materials
2	Capsule diamagnetism	$>$ 95% of B-field	Easy to meet
3	B_{in} / B_{out} at peak	$>$ 0.95	Set by soak-in time
4	ΔR_{wall}	$<$ 50 µm	Maintains drive symmetry
5	ΔT_{wall}	$<$ 2000 K	Maintains ignition quality DT layer
6	X-ray conversion	$>$ 95% of Au wall	Experimentally verified
7	Coil debris	Minimize mass, ensure melt	Determined by simulations and lab expts.
8	Coil movement	Allowed outside stay-out zones	Keep diagnostic views open

walls can begin to move inward leading to a displacement given by [8]

$$\Delta r = -\hat{r}\frac{B_0^2}{2\mu_0}\frac{\tau}{\rho_m\delta}\frac{\pi}{4\omega}. \quad (6)$$

Note that Δr is independent of wall thickness (as we saw with ΔT) but it is proportional to $1/\omega$ so that a faster pulser leads to a smaller wall displacement. A sufficiently slow pulser will generate a B-field pressure that is unable to overcome the buckling pressure of the hohlraum. In this case there is no wall motion. Estimating the wall motion with a 30 T B-field and using the temperature-dependent Au hohlraum gives an inward movement of about 300 µm.

The hohlraum wall is limited to a 2000 K increase in order to not risk melting any portion of the DT ice layer before the implosion. Thermal conduction from a 2000 K heated hohlraum wall through the gas is too slow to affect the capsule. However, radiative heat transfer from the hot wall, even for as short as $\sim$2 µs, poses a potential melt threat to the carefully grown DT fuel ice layer. Simulations using COMSOL [56] show that a wall temperature suddenly increased to 2000 K for 2 µs may cause a $\sim$1 µm layer of ice near the ablator to melt, creating a potential degradation to the implosion. Implosion simulations which include a 10 µm liquid DT region against the inner surface of the ablator show negligible performance degradation [57]. This project includes plans for an experiment in a surrogate geometry to benchmark the transient COMSOL thermal simulations with parameters close to the actual NIF experiment to verify the effect of thermal radiation on the capsule and DT ice layer.

Having ruled out Au as a possible hohlraum material for use with the fast pulser an estimate shows that a hohlraum resistivity of $\rho \geq 100\,\mu\Omega$-cm satisfies the first three requirements for a fast pulser ($\sim$2 µs rise-time) and a B-field up to 50 T. This created the need for a new hohlraum material which meets Requirements 3-6.

A parallel research effort exploring alternative hohlraum materials discovered that an alloy of 80% Ta and 20% Au atomic showed a resistivity of >100 x that of Au, exceeding the requirement of $\rho \geq 100\,\mu\Omega$-cm [58–61]. The choice of this alloy was guided by the Norbury-Linde rule, which says that alloys with large valence differences have more defects which result in increased electrical resistivity. The new hohlraums are made by co-sputtering Ta and Au onto a mandrel in the shape of the hohlraum. The resulting alloy has a glassy character to it. An overcoat of 120 µm epoxy for mechanical strength is placed on the coating and the mandrel is etched away making this coating process similar to how a Au hohlraum is made (apart from the epoxy). The sputter coating process creates some variability in the coating thickness depending on the angle between the surface normal and the source location so 15 µm was set as the nominal wall thickness. Typical NIF hohlraums use a 30-µm-thick gold wall (about the thickness of a human hair). A minimum wall thickness of 8 µm is required for a 6 to 7 ns NIF laser pulse to keep the X-ray diffusion front (Marshak wave) from breaking out of the exterior surface of the Au wall and reducing the capsule drive.

Figure 5b compares measurements of the B-field inside a finite length cylinder of $AuTa_4$ as current is applied to the wire solenoid surrounding the cylinder to measurements of the field without the $AuTa_4$ cylinder. The $AuTa_4$ cylinder was tested at a slightly lower current than the Au cylinder already discussed in Fig. 5a so the peak B-field is lower. This cylinder survives after the experiment and shows almost no difference between the B-field measured with or without the cylinder. The Au cylinder was broken into many small pieces.

Since the initial discovery of the Au:Ta alloy, research has developed coating techniques which can further increase the coating resistivity with better control of film microstructure and residual stress. In addition, coatings of $AuTa_xO_y$ and Au:Bi have been investigated. Oxygen containing $AuTa_xO_y$ alloys could have very high electrical resistivity of $>10^{10}\,\mu\Omega$-cm. The Au:Bi choice is the corresponding alloy of gold with a higher Z material that follows the Norbury-Linde rule.

X-ray Conversion

Requirement 6 assures that a new hohlraum material has nearly the same laser-to-X-ray conversion efficiency as pure Au so that any benefit of magnetization is not weakened by reduced X-ray drive. Radiation-hydrodynamic simulations show that a broad range of Au:Ta mixtures are equally effective at converting laser power to X-ray drive in the hohlraum as pure gold. Experiments performed on the Omega laser at the Laboratory for Laser Energetics (LLE) using laser drive on a foil for several different Au and Ta alloys show X-ray conversion within 95% of the pure Au result [62]. These results will be reported separately. The measurements and simulations also show m-band line emission at slightly lower energy than pure Au. Radiation hydrodynamic simulations which include a Tungsten doped capsule show that the m-band is absorbed in the Tungsten dopant and does not result in any significant pre-heat differences.

Coil Debris and Movement

Requirements 7 and 8 determine the size of Cu wire that can be used to generate the B-field. Requiring that the Cu wire melts just after peak current is considered necessary for mitigating the debris risk to the NIF optics or diagnostics [63, 64]. Given a fixed temperature increase to melt the radius of the wire scales as the fourth root of the current rise time, t_0 [65]. A fast pulser with a current rise of 2 microseconds using 26 gauge wire reaches melt in about 2 μs, near peak current. If the pulser were slowed to rise time of 1.25 ms (slower by 625 times) this would require a factor of 5 increase in wire radius which is a factor of 25 increase in the coil debris mass. This larger coil mass may require some type of kevlar netting (for example) placed next to the coil to mitigate the large amount of debris ejected toward the NIF optics and diagnostics. Measurements in an offline lab using 26 gauge wire show debris particles from exploded coils in the several to 20 μm size range when fully melted and in some cases as large as 500 μm when partially melted.

Energizing the Cu coil causes magnetic forces to axially compress and radially expand the coil. This movement has been observed in both experiment and modeling. Since the coil trajectory is not toward the hohlraum it does not mechanically influence the hohlraum wall motion. However, the coil motion eventually interferes with the line of sight of the equatorial diagnostics viewing the hot spot through hohlraum windows. This sets a maximum time allowed to reach peak current.

Additional Considerations

One additional consideration that is not a requirement but should be mentioned involves the shock wave launched in the hohlraum gas-fill during magnetization. Interferometry measurements inside a 5 mm diameter Cu cylinder during external magnetization show a converging cylindrical shock wave in the hohlraum fill gas that moves toward the capsule location. Wall heating alone is insufficient to create this shock [66]. ALE3D [67, 68] simulations reproduce the shock wave with a Au hohlraum and show that it is generated mostly by the sudden movement of the wall. At an applied field of $B = 30$ T simulations show that magnetization of a high electrical resistivity $AuTa_4$ hohlraum creates a gas density perturbation of only a few percent. However, for $B = 50$ T the simulated shock wave in a cryogenic hohlraum with 0.3 mg/cc of He gas-fill is stronger reaching a $\delta n_e / n_e \sim 0.2$. At the time in the simulations corresponding to the lasers firing for a NIF shot, the shock has not reached the capsule. The hohlraum gas-fill density is low enough that this shock only has a negligible effect on backscatter, refraction and X-ray drive symmetry.

Alternative Pulser Ideas

Given the above considerations we chose to use a fast pulser based on electronics like what is shown in Fig. 3 and combine it with a $AuTa_4$ hohlraum having $\geq 100\,\mu\Omega$-cm. This combination results in a solution that meets the Table I requirements. There were several other types of pulsers considered which were not selected but we believe it's helpful to describe these other options below.

For example, a slow pulser which ramps the external magnetic field in about 1 ms provides an option that can likely be used with a Au hohlraum. A slow pulser allows plenty of time to soak the B-field through the wall of a Au hohlraum and only increases the wall temperature a few hundred Kelvin. In addition, the inward wall pressure is below the buckling pressure for the cylindrical hohlraum so there is no wall motion. The wire size must increase significantly to hold off melt until peak current; this introduces some debris concerns which would need to be characterized and possibly mitigated. The energy storage required for the slow pulser is about 1 MJ (250 times the fast pulser).

Superconducting magnets are another option for magnetization. Magnets made of highly specialized conductors have achieved up to 45.5 T [69]. The conductors must be cooled to liquid He temperature and remain insulated from heat sources. The superconducting coils require cooling infrastructure which is bulky creating lots of potential to interfere with the required NIF laser beam and diagnostic lines of sight. In addition, the potential debris issues are significant. In light of these considerations we did not prioritize the superconducting magnet option for this project.

A third option considered is to combine the fast pulser with a slotted hohlraum. The slotted hohlraum uses a number of axial slots to disrupt the eddy currents and allow the B-field to diffuse more quickly to the inside of the hohlraum. Estimates based on the loop voltage across the slots and the Paschen breakdown voltage shows that a minimum of 4 evenly-spaced slots are required. ALE3D simulations show that there must be at least 16 slots to sufficiently disrupt the eddy currents and meet the wall motion and heating requirements. A hohlraum design with sixteen or more slots is significantly challenging so this option was deprioritized.

Pulser for Cryogenic Implosions

The pulser currently in use for all NIF magnetized room temperature experiments, which include implosions, gas-pipes, Discovery Science experiments and X-ray source development, can achieve a peak field of about 30 to 35 T and is adequate for magnetizing room temperature gas-filled capsule implosions. However, to test the effect of magnetization on cryogenic DT-layered targets a new pulser integrated into the NIF cryogenic target positioner and capable of ~ 50 T is required. The new pulser is under construction and will be located outside the target bay in the switchyard to reduce the risk of neutron damage. The current is transported through the cryogenic target positioner to the target with a combination of coax cables and striplines. Figure 4b shows that the magnetized DT ice layer targets will use a two-layer coil on each half of the hohlraum to achieve the higher field. Thermal simulations show that the coil and hohlraum temperatures must be independently controlled to obtain the spherically symmetric isotherms required to obtain an ignition quality DT ice layer.

Future Plans

The first NIF magnetized implosions have started and use room temperature targets with neo-pentane (C_5H_{12}) at 60 Torr for the hohlraum gas-fill and pure D_2 at 18,000 Torr as the capsule fill. These experiments will quantify the magnetization effect on the neutron yield and ion temperature. Simulations predict an increase of 1 keV ($\sim$ 35%) in the ion temperature and a factor of 1.6 to 2 increase in the yield. Energy spectra measurements of the 2.45 MeV primary neutrons will show both the change in yield and ion temperature. Comparing the experiments to simulations will quantify the effect of magnetization on performance.

Clues to the magnitude of the compressed hot-spot B-field will be found by analyzing the secondary neutron spectral data. The primary yield from D–D nuclear reactions generates isotropic 2.45 MeV neutrons and 1.01 MeV tritons. The tritons can then react with D generating secondary neutrons at 14.1 MeV. The neutron spectra from a magnetized implosion may be different when measured along the B-field direction or orthogonal to it [70]. If the hot-spot B-field is sufficiently amplified a triton can be trapped in the hot spot provided its Larmour radius ($\rho_L = v_T/\Omega_c$ where v_T is the triton speed at 1.1 MeV and Ω_c is the cyclotron frequency of the triton) is less than the hot-spot radius. Secondary neutron spectral measurements on SNL's MagLIF project have shown differences in the secondary neutron energy spectra along and across the B-field which have been used to estimate the internal (compressed) B-field [71, 72]. In general, the secondary spectra are affected by both the local B-field and the total ρR and will require analysis to separate out the effects from each other.

Interpreting the magnetized hot-spot shape will require new analysis methods since it can be affected by hot-spot physics as well as the hohlraum drive. Capsule modeling using a spherically symmetric X-ray drive shows that the $J \times B$ force on the plasma is outward (adding to the kinetic pressure) and stronger at the equator than the poles tending to make the hot-spot shape oblate [39]. But a second effect caused by greater thermal conduction to the poles than the equator causes more ablation at the poles and subsequently a larger pole radius tending to make the hot spot prolate. In addition to these capsule effects the B-field may modify the cross-beam energy transfer [73–75] or affect the conversion of laser power to X-ray drive. Both of these effects can alter the symmetry of the X-ray drive generated from inside the hohlraum and can lead to an asymmetry in the hot-spot shape at stagnation. We will need to rely on experiments to determine the relative significance of each of these effects.

The planned magnetized cryogenic DT-layered implosion design is selected on the basis of its demonstrated reproducibility and robustness in unmagnetized NIF experiments [76, 77]. If magnetization proves effective, we will develop new implosion designs that fully leverage the magnetic-field-induced enhancement. This could entail adding a magnetic field to several of the best-performing NIF platforms or something quite different. We expect a magnetic field to create the possibility to push a range of implosion designs closer to, or into, the ignition and high fusion-energy-gain regime.

Conclusions

In conclusion, application of a seed magnetic field to indirect drive implosions on NIF is an ongoing project with a number of science and technology challenges. Expectations based on simulations are that the B-field should lead to a factor of 2 increase in yield and $\sim$ 35% increase in the ion temperature. Once demonstrated, magnetization can be used to assist many ignition designs. The discovery of a high electrical resistivity $AuTa_4$ alloy with laser to X-ray conversion very close to Au has led us to a design choice of a fast pulser with the new hohlraum material. This can meet the requirements for magnetization outlined in Table 1. We have carefully considered a number of physics issues in the context of magnetization and described the design choices we've made to respond to them. Magnetized implosion experiments have now begun and we will describe the result in a separate article.

Acknowledgements This work was performed under the auspices of the U.S. Department of Energy by Lawrence Livermore National Laboratory under Contract DE-AC52-07NA27344 and by the LLNL-LDRD program under Project Number 20-SI-002.

Data Availibility The data that supports the findings of this study are available within the article [and its supplementary material].

References

1. A.L. Kritcher, A.B. Zylstra, D.A. Callahan et al., Achieving record hot spot energies with large HDC implosions on NIF in HYBRID-E. Phys. Plasmas (2021). https://doi.org/10.1063/5.0047841
2. A. Zylstra, O. Hurricane et al., Burning plasma achieved in inertial fusion. Nature **601**, 542 (2022). https://doi.org/10.1038/s41586-021-04281-w
3. A. Kritcher, C. Young, H. Robey et al., Design of inertial fusion implosions reaching the burning plasma regime. Nat. Phys. (2022). https://doi.org/10.1038/s41567-021-01485-9
4. J.S. Ross, J.E. Ralph, A.B. Zylstra, A.L. Kritcher, H.F. Robey, C.V. Young, O.A. Hurricane, et al., Experiments conducted in the burning plasma regime with inertial fusion implosions. Nat. Commun. (2021)
5. J.G. Linhart et al., Amplification of magnetic fields and heating of plasma by a collapsing metallic shell. Nucl. Fusion Suppl. **2**, 733 (1962)
6. L.J. Perkins et al., The potential of imposed magnetic fields for enhancing ignition probability and fusion energy yield in indirect-drive inertial confinement fusion. Phys. Plasmas **24**, 062708 (2017)
7. J.D. Moody, Boosting inertial-confinement-fusion yield with magnetized fuel. Am. Phys. Soc. **14**, 51 (2021). https://doi.org/10.1103/Physics.14.51
8. J.D. Moody et al., Transient magnetic field diffusion considerations relevant to magnetically assisted indirect drive inertial confinement fusion. Phys. Plasmas **27**, 112711 (2020)
9. S.I. Braginskii, in *Reviews of Plasma Physics*, ed. by M.A. Leontovich, vol. 1 (Consultants Bureau, New York, 1965), p. 205
10. J.D. Sadler, H. Li, K.A. Flippo, Parameter space for magnetization effects in high-energy-density plasmas. Matter Radiat. Extrem. **6**, 0659902 (2021)
11. B. Bigot, Nucl. Fusion (2019). https://doi.org/10.1088/1741-4326/ab0f84
12. X. Yuhong, Matter Radiat. Extrem. **1**, 192 (2016). https://doi.org/10.1016/j.mre.2016.07.001
13. M.R. Gomez et al., Experimental demonstration of fusion-relevant conditions in magnetized liner inertial fusion. Phys. Rev. Lett. **113**, 155003 (2014)
14. M.R. Gomez et al., Performance scaling in magnetized liner inertial fusion experiments. Phys. Rev. Lett. **125**, 155002 (2020)
15. D.H. Barnak, J.R. Davies, R. Betti, M.J. Bonino, E.M. Campbell, VYu. Glebov et al., Phys. Plasmas **24**, 056310 (2017)
16. J.R. Davies et al., Laser-driven magnetized liner inertial fusion. Phys. Plasmas **24**, 062701 (2017)
17. J.W. Mather, Phys. Fluids **8**, 366 (1965)
18. A. Schmidt, V. Tang, D. Welch, Phys. Rev. Lett. **109**, 205003 (2012)
19. U. Shumlak, J. Chadney, R.P. Golingo, D.J. Den Hartog, M.C. Hughes, S.D. Knecht, W. Lowrie, V.S. Lukin, B.A. Nelson, R.J. Oberto, J.L. Rohrbach, M.P. Ross, G.V. Vogman, The sheared-flow stabilized Z-pinch. Fusion Sci. Technol. **61**(1T), 119–124 (2012). https://doi.org/10.13182/FST12-A13407
20. I.R. Lindemuth, R.E. Siemon, Am. J. Phys. **77**, 407 (2009). https://doi.org/10.1119/1.3096646
21. J.D. Lawson, Some criteria for a useful thermonuclear reactor. Tech. Rep. GP/R 1807, Atomic Energy Research Establishment. https://www.euro-fusion.org/fileadmin/user_upload/Archive/wp-content/uploads/2012/10/dec05-aere-gpr1807.pdf (1955)
22. J.D. Lawson, Proc. Phys. Soc. B **70**, 6 (1957)
23. R. Betti, P.Y. Chang, B.K. Spears, K.S. Anderson, J. Edwards, M. Fatenejad, J.D. Lindl, R.L. McCrory, R. Nora, D. Shvarts, Phys. Plasmas (2010). https://doi.org/10.1063/1.3380857
24. P.Y. Chang, R. Betti, B.K. Spears, K.S. Anderson, J. Edwards, M. Fatenejad, J.D. Lindl, R.L. McCrory, R. Nora, D. Shvarts, Generalized measurable ignition criterion for inertial confinement fusion. Phys. Rev. Lett. (2010). https://doi.org/10.1103/PhysRevLett.104.135002
25. O.A. Hurricane, S.A. Maclaren, M.D. Rosen, J.H. Hammer, P.T. Springer, R. Betti, Phys. Plasmas (2021). https://doi.org/10.1063/5.0035583
26. S.E. Wurzel, S.C. Hsu, Progress toward fusion energy breakeven and gain as measured against the Lawson criterion. arXiv:2105.10954
27. S. Atzeni, J. Meyer-ter-Vehn, *The Physics of Inertial Fusion* (Oxford University Press, Oxford, 2004)
28. B. Cheng, T.J.T. Kwan, Y.-M. Wang, S.H. Batha, On thermonuclear ignition criterion at the National Ignition Facility. Phys. Plasmas **21**, 102707 (2014). https://doi.org/10.1063/1.4898734
29. J.D. Lindl, *Interital Confinement Fusion: The Quest for Ignition and Energy Gain Using Indirect Drive* (Springer, New York, 1998)
30. J. D. Lindl et al., The physics basis for ignition using indirect-drive targets on the National Ignition Facility. Phys. Plasmas **11**, 339 (2004)
31. H.-S. Bosch, G.M. Hale, Improved formulas for fusion cross-sections and thermal reactivities. Nucl. Fusion **32**, 611 (1992)
32. O.A. Hurricane et al., Beyond alpha-heating: driving inertially confined fusion implosions toward a burning-plasma state on the National Ignition Facility. Plasma Phys. Control. Fusion **61**, 014033 (2018)
33. M. Hohenberger, P.-Y. Chang, G. Fiksel, J.P. Knauer, R. Betti, F.J. Marshall, D.D. Meyerhofer, F.H. Séguin, R.D. Petrasso, Inertial confinement fusion implosions with imposed magnetic

field compression using the OMEGA Laser. Phys. Plasmas (2012). https://doi.org/10.1063/1.3696032
34. S. Le Pape, L.F. Berzak Hopkins, L. Divol, A. Pak, E.L. Dewald, S. Bhandarkar, L.R. Bennedetti, T. Bunn, J. Biener, J. Crippen et al., Fusion energy output greater than the kinetic energy of an imploding shell at the National Ignition Facility. Phys. Rev. Lett. **120**, 245003 (2018)
35. D.D.-M. Ho, L.J. Perkins, G.B. Zimmerman, G. Kagan, J.D. Salmonson, B G. Logan, D.T. Blackfield, M.A. Rhodes, 58th Annual Meeting of the APS Division of Plasma Physics, CO8.00001 (2016)
36. S. Yu. Gus'kov et al Sov. J. Quantum Electron. (1984)
37. G. Zimmerman, W.L. Kruer, Numerical simulation of laser-initiated fusion. Comments Plasma Phys. Control. Fusion **2**, 85 (1975)
38. J. Nuckolls, L. Wood, A. Thiessen, G.B. Zimmerman, Nature **239**(5368), 139–142 (1972)
39. D.D.-M. Ho, G.B. Zimmerman, A.L. Velikovich, R.M. Kulsrud, J.D. Moody, T. Woods, P.A. Amendt. 62nd Annual Meeting of the APS Division of Plasma Physics CO05.00011 (2020)
40. R.P. Drake, J.H. Hammer, C.W. Hartman, L.J. Perkins, D.D. Ryutov, Submegajoule liner implosion of a closed field line configuration. Fusion Technol. **30**, 310–325 (1996)
41. I.R. Lindemuth et al., Magnetic-compression/magnetized-target fusion MAGO/MTF: a marriage of inertial and magnetic confinement. In: IAEA Conference Proceedings IAEA-CN-64/DP-27, 16th International Conference on Fusion Energy, Montreal, pp. 723–724 (1996)
42. P.J. Turchi, Imploding liner compression of plasma: concepts and issues. IEEE Trans. Plasma Sci. **36**, 52–61 (2008)
43. L.J. Perkins, B.G. Logan, G.B. Zimmerman, C.J. Werner, Phys. Plasmas **20**, 072708 (2013)
44. S.A. Slutz et al., Pulsed-power-driven cylindrical liner implosions of laser preheated fuel magnetized with an axial field. Phys. Plasmas **17**, 056303 (2010)
45. C.A. Walsh et al., Nucl. Fusion **60**, 106006 (2020)
46. C.A. Walsh, Magnetized ablative Rayleigh–Taylor instability in 3-D. Phys. Rev. E **105**, 025206 (2022)
47. O.V. Gotchev, P.Y. Chang, J.P. Knauer, D.D. Meyerhofer, O. Polomarov, J. Frenje, C.K. Li, M.J.-E. Manuel, R.D. Petrasso, J.R. Rygg, F.H. Séguin, R. Betti, Laser-driven magnetic-flux compression in high-energy-density plasmas. Phys. Rev. Lett. (2009). https://doi.org/10.1103/PhysRevLett.103.215004
48. J.P. Knauer et al., Compressing magnetic fields with high-energy lasers. Phys. Plasmas **17**, 056318 (2010)
49. P.Y. Chang, G. Fiksel, M. Hohenberger, J.P. Knauer, R. Betti, F.J. Marshall, D.D. Meyerhofer, F.H. Séguin, R.D. Petrasso, Fusion yield enhancement in magnetized laser-driven implosions. Phys. Rev. Lett. (2011). https://doi.org/10.1103/PhysRevLett.107.035006
50. A. Nishiguchi, T. Yabe, M.G. Haines, Nernst effect in laser-produced plasmas. Phys. Fluids **28**, 3683 (1985)
51. D.J. Strozzi, L.J. Perkins, M.M. Marinak, D.J. Larson, J.M. Koning, B.G. Logan, J. Plasma Phys. **81**, 475810603 (2015)
52. D.S. Montgomery, B.J. Albright, D.H. Barnak, P.Y. Chang, J.R. Davies, G. Fiksel, D.H. Froula, J.L. Kline, M.J. MacDonald, A.B. Sefkow, L. Yin, R. Betti, Use of external magnetic fields in Hohlraum plasmas to improve laser-coupling. Phys. Plasmas (2015). https://doi.org/10.1063/1.4906055
53. P. Clark Souers, Hydrogen Properties for Fusion Energy, University of California Press, Berkeley, Chapters 16 and 17 (1986)
54. J.D. Jackson, *Classical Electrodynamics*, 2nd edn. (Wiley, New York, 1975), p. 199
55. S.W. Haan, J.D. Lindl, D.A. Callahan et al., Point design targets, specifications, and requirements for the 2010 ignition campaign on the National Ignition Facility. Phys. Plasmas (2011). https://doi.org/10.1063/1.3592169
56. COMSOL Multiphysicsl® v. 5.6. www.comsol.com. COMSOL AB, Stockholm
57. D. Ho, Private Communication
58. A. Engwall et al., U.S. Patent Application No. 62/928968 (October 31, 2019) Lawrence Livermore National Security, LLC, "High-resistivity metal alloy coatings fabricated with physical vapor deposition."
59. L.B. BayuAji, A.M. Engwall, J.H. Bae, A.A. Baker, J.L. Beckham, S.J. Shin, X. LeproChavez, S.K. McCall, J.D. Moody, S.O. Kucheyev, Sputtered Au-Ta films with tunable electrical resistivity. J. Phys. D **54**, 075303 (2021)
60. A.M. Engwall, L.B. BayuAji, A.A. Baker, S.J. Shin, J.H. Bae, S.K. McCall, J.D. Moody, S.O. Kucheyev, Effect of substrate tilt on sputter-deposited $AuTa_4$ films. Appl. Surf. Sci. **547**, 149010 (2021). https://doi.org/10.1016/j.apsusc.2021.149010
61. J.H. Bae, L.B. Bayu Aji, S.J. Shin, A.M. Engwall, M.H. Nielsen, A.A. Baker, S.K. McCall, J.D. Moody, S.O. Kucheyev, Gold-tantalum alloy films deposited by high-density-plasma magnetron sputtering. J. Appl. Phys. **130**, 165301 (2021)
62. H. Sio et al., X-ray conversion efficiency of Au-Ta alloys. manuscript in preparation
63. D.C. Eder, A.C. Fisher, A.E. Koniges, N.D. Masters, Modelling debris and shrapnel generation in inertial confinement fusion experiments. Nucl. Fusion **53**, 113037 (2013)
64. N. D. Masters, A. Fisher, D. Kalantar, J. Stölken, C. Smith, R. Vignes, S. Burns, T. Doeppner, A. Kritcher, H-S. Park, Debris and shrapnel assessments for National Ignition Facility targets and diagnostics. J. Phys.: Conference Series, Volume 717, 9th International Conference on Inertial Fusion Sciences and Applications (IFSA 2015) 20-25 September 2015, Seattle
65. We approximate the current rise as a linear ramp to I_0 in time t_0 and specify the coil wire cross-sectional area A, length L and resistivity ρ. This gives a wire resistance of $\rho L/A$ and total Ohmic heating energy of $I_0^2 \frac{t_0}{3}\frac{\rho}{A}$. This energy heats a wire mass proportional to the coil volume AL. The temperature increase of the coil scales as $\Delta T \sim I_0^2 \frac{t_0}{A^2}$. Given a fixed temperature increase to melt the radius of the wire is seen to scale as the fourth root of the current rise time, t_0
66. Y. Sone, J. Phys. Soc. Jpn. **20**, 222 (1965)
67. A.L. Nichols, ALE-3D user's manual, Technical Report No. UCRL-MA- 152204 (Lawrence Livermore National Laboratory, 2007)
68. R.N. Rieben et al., An arbitrary Lagrangian–Eulerian discretization of MHD on 3D unstructured grids. J. Comput. Phys. **226**(1), 534–570 (2007)
69. S. Hahn et al., Nature **570**, 496 (2019). https://doi.org/10.1038/s41586-019-1293-1
70. H. Sio, J.D. Moody, D.D. Ho, B.B. Pollock, C.A. Walsh, B. Lahmann, D.J. Strozzi, G.E. Kemp, W.W. Hsing, A. Crilly, J.P. Chittenden, B. Appelbe, Rev. Sci. Instrum. (2021). https://doi.org/10.1063/5.0043381
71. P.F. Schmit et al., Understanding fuel magnetization and mix using secondary nuclear reactions in magneto-inertial fusion. Phys. Rev. Lett. **113**, 155004 (2014)
72. P.F. Knapp et al., Effects of magnetization on fusion product trapping and secondary neutron spectra. Phys. Plasmas **22**, 056312 (2015)
73. W.L. Kruer, S.C. Wilks, B.B. Afeyan, S. Kirkwood, K. Robert, Energy transfer between crossing laser beams. Phys. Plasmas **3**, 382385 (1996)

74. P. Michel et al., Tuning the implosion symmetry of ICF targets via controlled crossed-beam energy transfer. Phys. Rev. Lett. **102**, 025004 (2009)
75. J.D. Moody et al., Multistep redirection by cross-beam power transfer of ultrahigh-power lasers in a plasma. Nat. Phys. **8**, 344 (2012)
76. C.A. Thomas, E.M. Campbell, K.L. Baker, D.T. Casey, M. Hohenberger, A.L. Kritcher, B.K. Spears, S.F. Khan, R. Nora, D.T. Woods, J.L. Milovich, R.L. Berger, D. Strozzi, D.D. Ho, D. Clark, B. Bachmann, L.R. Benedetti, R. Bionta, P.M. Celliers, D.N. Fittinghoff, G. Grim, R. Hatarik, N. Izumi, G. Kyrala, T. Ma, M. Millot, S.R. Nagel, P.K. Patel, C. Yeamans, A. Nikroo, M. Tabak, M. Gatu Johnson, P.L. Volegov, S.M. Finnegan, Phys. Plasmas **27**, 112–708 (2020). https://doi.org/10.1063/5.0019193
77. K.L. Baker et al., High-performance indirect-drive cryogenic implosions at high adiabat on the National Ignition Facility. Phys. Rev. Lett. **121**, 135001 (2018)